Mechanism for Long Photocurrent Time Constants in α-Ga_2O_3 UV photodetectors

A.Y. Polyakov[1], A.V. Almaev[2], V.I. Nikolaev[1, 3], A.I. Pechnikov[1,3], V.I. Shchemerov[1], A.A. Vasilev[1], E.B. Yakimov[1, 4], A.I. Kochkova[1], V.V. Kopyev[2], B.O Kushnarev[2] and S. J. Pearton[5*]

[1.]National University of Science and Technology MISiS, Moscow, Leninsky pr. 4, Moscow 119049, Russia

[2]Tomsk State University, 36 Lenin Avenue, Tomsk, 634050, Russia

[3.] Perfect Crystals LLC, 38k1 Toreza Avenue, off.213, Saint Petersburg, 194223, Russia

[4.] Institute of Microelectronics Technology and High Purity Materials, Russian Academy of Sciences, 6 Academician Ossipyan str., Chernogolovka, Moscow Region 142432, Russia

[5.] Department of Materials Science and Engineering, University of Florida, Gainesville, FL 32611

*Corresponding author, E-mail: spear@mse.ufl.edu

ABSTRACT

Deep centers and their influence on photocurrent spectra and transients were studied for interdigitated photoresistors on α-Ga_2O_3 undoped semi-insulating films grown by Halide Vapor Phase Epitaxy (HVPE) on sapphire. Characterization involving current-voltage measurements in the dark and with monochromatic illumination with photons with energies from 1.35 eV to 4.9 eV, Thermally Stimulated Current (TSC), Photoinduced Current Transients Spectroscopy (PICTS) showed the Fermi level in the dark was pinned at E_c-0.8 eV, with other prominent centers being deep acceptors with optical thresholds near 2.3 eV and 4.9 eV and deep traps with levels at E_c-0.5 eV, E_c-0.6 eV. Measurements of photocurrent transients produced by illumination with photon energies 2.3 eV and 4.9 eV and Electron Beam Induced Current (EBIC) imaging point to the high sensitivity and external quantum efficiency values being due to hole trapping enhancing the lifetime of electrons and inherently linked with the long photocurrent transients. The photocurrent transients are stretched exponents, indicating the strong contribution of the presence of centers with barriers for electron capture and/or of potential fluctuations.

The wide-bandgap semiconductor Ga_2O_3 is currently under intense study because of the great promise for use in high-power devices and solar-blind UV photodetectors [1-14]. For power devices, the main advantages of Ga_2O_3 are due to the electric breakdown field exceeding by several times the breakdown field of III-Nitrides or SiC due to the large bandgap of ~5 eV [1-11]. Additionally, the thermodynamically stable monoclinic β-Ga_2O_3 polymorph allows economic growth of high-quality substrate material from the melt, applicability of all major epitaxial techniques to growth of device-quality epilayers, while the metastable corundum structure α-Ga_2O_3 can be epitaxially grown on cheap isomorphic α-Al_2O_3 sapphire substrates and can be utilized to create heterojunctions with a wide range of corundum structured oxides of Al, In, or transition metals and rare metals [1-6, 9,15].

For photodetectors, the advantages are the wide bandgap and a low density of deep centers, which makes the material solar-blind, with high photosensitivity [2, 3, 7, 8, 10, 13]. The external quantum efficiency of Ga_2O_3 photodetectors demonstrates an unusually high gain, not uncommonly exceeding 10^1-10^5 [3]. Unfortunately, such high gain is often accompanied by long photocurrent build-up and decay times on the order of many seconds, which is a problem for practical applications [16]. Possible explanations or the observed phenomena in β-Ga_2O_3 Schottky diodes include 1) the effect is due to charges multiplication by impact ionization [17], 2) assigning the high photosensitivity to the polaronic nature of holes in Ga_2O_3, making them virtually immobile and contributing to changes of the Schottky barrier height under illumination [18], or 3) to trapping of holes on abundant deep hole traps thus changing the effective Schottky barrier height and producing an anomalously high photocurrent [19, 20]. Hypotheses 2 and 3 suggest the nature of photocurrent in Schottky diodes of β-Ga_2O_3 is totally different from usual photodiodes and comes from build- up of charge either on polaronic self-trapped holes or on deep hole traps, the anomalously high photocurrent being the result of Schottky barrier height decrease under illumination. The natural consequence is the long-time scale of the photocurrent transients because of the necessity to dissolve the immobile charge created by light in the space

charge region by either thermally activated holes removal or by interaction with residual electrons flowing through the space charge region and creating dark current [20].

We have presented experimental evidence in favor of model 3 by analyzing the effects on photocurrent of irradiation with high energy particles [20]. However, the unusually high photosensitivity and long build-up and decay times of photocurrent have been also reported for photoconductor structures with closely spaced interdigitated Ohmic contacts and these effects have been observed for both β-Ga_2O_3 and α-Ga_2O_3 and even polycrystalline rhombohedral κ-Ga_2O in electric fields inconsistent with the impact ionization hypothesis 1 [21, 22].

In this paper we present results of photocurrent build-up and decay for photoconductors with interdigitated Ohmic contacts patterns on undoped α-Ga_2O_3. We suggest the photoconductivity time constants are due to photoelectrons in the presence of strong trapping of holes.

The undoped α-Ga_2O_3 films were prepared by Halide Vapor Phase Epitaxy (HVPE) on basal plane sapphire at 500ºC, with GaCl being formed in-situ by interaction with HCl flowing over the liquid Ga crucible and serving as the Ga precursor transported into the reaction zone. Oxygen was supplied in the form of ultra-pure O_2. The VI/III mole flow ratio was 4.2, spectrally clean argon was used as a carrier gas to keep the total gas flow rate through the reactor at 10 slm. The growth rate was 2.4 μm/h, with total thickness of the films of 5 μm. The layers were pure α-Ga_2O_3 with (0001) orientation and no admixture of other polymorphs, as proved by x-ray diffraction (XRD) patterns. The Full Width at Half Maximum (FWHM) of the (0004) reflection measured in the double-crystal XRD geometry was 14 arcminutes. The growth procedure has been described in detail elsewhere [23, 24]. The electrical properties, deep trap spectra and Positron Annihilation Spectra (PAS) of similarly grown films were reported previously [25].

The photoconductors with an interdigitated contact pattern were fabricated by by e-beam deposition of Ti/Ni (100 nm/100 nm) contacts and lithographic lift-off to form a structure with fingers 10 μm wide and 1 mm long with distance between the fingers of 30 or 50 μm, with total number of fingers of 75 or 50. The fingers on the opposite sides were connected by the common

Ti/Ni bus, and contact pads for probing were fabricated. The general schematics of the structure with the distance between the fingers of 30 μm is illustrated in Fig. 1. These samples were used for characterization of the spectral monochromatic current photosensitivity S_I, spectral detectivity D^*, and external quantum efficiency EQE.

The obtained photosensitivity and EQE for measurements performed on the structures with interdigital distances of 30 μm and 50 μm (shown as Fig. S1(a, b) and Fig. S2(a, b) of the Supplementary Material). The graphs in Fig. S1, S2 were obtained with applied voltage of 10V. The dependence of the photosensitivity and EQE on applied voltage is shown in Fig. S3(a, b**),** built for the photodetector with interdigital distance of 30 μm. The spectral current photosensitivity peaked at 235 nm, in good agreement with the known value of α-Ga_2O_3 bandgap of 5.2-5.3 eV [1]. The peak photosensitivity and EQE measured at 10V were, respectively, 7×10^4 A/W and 3.8×10^5 (the 30 μm sample) and 700 A/W, 3800 (the 50 μm sample). The photosensitivity and EQE considerably increased with applied voltage from 10 V to 40 V, as illustrated in Fig. S3(a, b) of the Supplementary Material.

We focus here on the electrical properties of the 30 μm sample, including the deep trap spectra and the kinetics of photocurrent measured at 300, 340 and 380 K with almost band edge excitation with 4.8 eV photons and below-bandgap excitation with 2.3 eV photons. The characterization included dark current versus voltage (I-V), I-V characteristics measured with monochromatic illumination with a set of Light Emitting Diodes (LEDs) with peak photon energies from 1.35 eV (wavelength of 940 nm) to 4.8 eV (wavelength of 259 n -the optical power output densities of 250 mW/cm^2 for photon energies of up to 3.4 eV (365 nm wavelength), 15 mW/cm^2 for the photon energy of 4.5 eV (277 nm), and 1.2 mW/cm^2 for photon energy of 4.8 eV (259 nm)), current versus temperature (I-T) measurements at fixed voltage in the dark and after illumination with monochromatic light (Thermally Stimulated Current (TSC) [26], Photoinduced Current Transient (PICTS) [27], Scanning Electron Microscope (SEM) images taken in the secondary electrons (SE) mode and in Electron Beam Induced Current

(EBIC) mode. With Ohmic contacts, the EBIC signal is produced as a result of local excessive charge generation and local increase of "photocurrent" that is determined by the local area of charge generation and applied bias. The one-dimensional theory reported for estimation of diffusion length of nonequilibrium charge carriers in HgCdTe detectors was employed [28,29].

The experimental setups used have been described previously [23, 24, 30- 32]. The kinetics of photocurrent build-up and decay were measured at 300, 340 and 380K using a B2902A current/ voltage meter (Keysight Technologies, USA), allowing to drive the LED used for photocurrent excitation using one output of the device and collect the photocurrent values variations with time at fixed applied voltage using the second output. The data could be collected with time step varying from 0.2 ms at the beginning of the process to 100 ms at longer times, so that relaxation times from 0.2 ms to 10000 s could be monitored simultaneously and the data collected for several consecutive build-up and decay measurements. The digitized data was used to build the time dependence of the photocurrent dI/dln(t) versus logarithm of time, ln(t) graph. Fitting of the observed relaxation processes was achieved with either assuming simple exponential decays or stretched exponents of the form $I=I_o\exp(-(t/\tau)^{\beta})$ [33, 34]. The procedure is similar to that used to analyze current relaxations in AlGaN/GaN High Electron Mobility Transistors (HEMTs) [35].

We start with room temperature measurements of I-V characteristics measured in the dark and with monochromatic illumination. Fig. 2(a) shows the raw I-V data and Fig. 2(b) presents the photocurrent spectra for two voltage polarities. The dark current is low, the photocurrent spectra for both voltage directions show two well defined optical thresholds near 2.3 eV and 3.1 eV, the apparent fall of photosensitivity spectra at the highest photon energies used (259 nm, 4.8 eV) is the result of much lower power output density for the LEDs with wavelengths 277 nm and 259 nm.

After the spectra measurements, the devices were heated at -40V to 430K, cooled down to 120K at -40V at cooling rate 1.5 K/min while measuring the current, then illuminated at 120K

and -40V with the 4.8 eV LED for 5 minutes and after that heated at a rate of 1.5 K/min at -40V while measuring the current. Fig. 3 shows the evolution of the I-T dependence after such cycle. In the cooling down I-T curve, there high temperature region of exponential growth of current with temperature with activation energy of 0.8 eV, then, at lower temperatures, two peaks near 350K and 250K. These peaks are likely due to the contribution of deep centers recharged during the spectral measurements and not fully discharged even after heating up to 430K. According to the theory of TSC [26], the activation energy E_a of the peak in TSC can be estimated as approximately $E_a=k_BT_{peak}\times\ln(T_{peak}^4/\alpha)$ [26], where k_B is the Boltzmann constant, T_{peak} is the peak temperature and α is the heating rate. This converts to $E_a\sim23\times k_B\times T_{peak}$. Then corresponding activation energies are 0.7 eV and 0.5 eV. In the heating up curve, the peaks observed are due to centers with activation energies 0.25 eV, 0.35 eV, 0.5 eV, 0.6 eV. The reason the current collapses at temperatures between 200 and 230K is not clear. The peaks detected are the usual deep traps observed in the upper half of the bandgap of lightly doped α-Ga_2O_3 films [23, 24].

These measurements were repeated 24 hours later after heating up the sample at -40V to 430K, cooling down to 140K at -40V while measuring current, shining 4.8 eV light for 5 minutes at 140K and measuring current at -40V while heating the sample up in the dark after illumination. In this second TSC experiment, the exponential region with activation energy 0.8 eV extends in the cooling down branch all the way down to 250K with no steps due to 0.7 eV and 0.5 eV traps. In the heating up branch measured after illumination at 140K, the peaks due to the 0.25 eV and 0.35 eV traps are not observed while the magnitude of the 0.5 eV and 0.6 eV peaks are significantly diminished. The current collapse observed in the first run does not occurring at 170K and extends to 230K. The conclusions from these TSC experiments is that the Fermi level in the dark is located at E_c-0.8 eV, centers in the upper half of the bandgap near E_c-0.25, E_c-0.35, E_c-0.5, E_c-0.6 eV can effectively trap electrons, and that the process of releasing electrons from these electron traps is lengthy. The data of Fig. 2(b) also indicates the presence of

deep acceptors with optical ionization energies 2.3 eV and 3.1 eV in addition to the host of electron traps in the upper half of the bandgap. Additional experiments performed with 2.3 eV (530 nm peak wavelength) LED excitation and 4.5 eV excitation produce similar results.
A PICTS spectrum measured at -10V bias and 4.8 eV LED excitation is shown in Fig. 4. Two peaks are seen with activation energy 0.5 eV and 0.7 eV, similar to those detected in TSC.

The results of SEM/EBIC measurements were revealing. With applied external bias, the EBIC signal distribution was observed, and the magnitude increased with applied bias. Fig. 5(a) presents the EBIC image collected with 25 keV, 10 nA probing beam excitation with no applied bias. Fig. 5(b) is the image taken with 10V applied bias between the contact pads, Fig. 5 (c) is taken with 20V bias, and Fig. 5(d) is the blow-up of the Fig. 5(c) image taken with a higher magnification. Excessive charge can definitely travel all the way between the contact fingers even when it is generated at quite a distance from them, although there are dark regions where current flow far away from the fingers is not efficient (dark regions in Fig. 5(d). It is also be noted that a) measurable contrast could only be detected with high enough probing beam current (in general beam currents > 10 nA) and b) after the exposure of the device to high applied voltage between the pads and high probing current, a wait of many hours in the dark was required before the same EBIC image could be reproduced. The diffusion length of nonequilibrium charge carriers even in the best quality β-Ga_2O_3 films grown by HVPE on native substrates does not exceed 0.6 μm [15] and, for α-Ga_2O_3 is about an order of magnitude lower [23, 24]. Since the amplitude of EBIC signal observed is orders of magnitude higher than expected knowing the generation volume of the excessive charge distribution and the number of electron-hole pairs produced by the probing beam electrons [20, 36] we conclude photocurrent amplification is occurring.

Further understanding is provided by analysis of kinetics of the photocurrent build-up and decay for the 4.8 eV (259 nm) LED excitation (almost band-edge excitation) and 2.3 eV LED excitation (below-bandgap excitation corresponding to strong increase of photocurrent (Fig. 2).

The schematic of the experiment is illustrated by Fig. 6. At three temperatures, a train of LED excitation pulses 1000 s long with 1000-2000 s interval between the pulses was applied and for each pulse the relaxation curves were analyzed by building the dependence of dI(t)/d(ln(t)). In Ref. [27] we show that for exponential decays of the form $I=I_o\exp(-t/\tau)$, such presentation produces peaks at $t=\tau$, so that the number of peaks allows to determine the number of characteristic processes with different relaxation times and to obtain the characteristic τ values for each process. In the presence of potential fluctuations and/or barriers for capture of charge carriers the relaxation curves can take the form of stretched exponents $I=I_o\exp(-(t/\tau)^{\mu})$, with the broadening parameter β related to the magnitude of potential fluctuations or the fluctuations of the capture barrier value. In this case, the differentiation by ln(t) produces peaks at $t=\tau$, but the peaks are asymmetrically broadened compared to the case of simple exponents. The value of the broadening parameter β can then be estimated by either directly fitting the observed form of the peak in the first derivative by ln(t) or from the ratio of the first and second derivatives by ln(t) and the halfwidth of the first derivative on the high t side of the curve [35].

The characteristic features of relaxations in Fig. 6 are as follows. For 4.8 eV (259 nm) LED excitation, the photocurrent build-up is at first relatively fast, passes through a maximum, and then, for very long pulse times, shows a slight decrease. With each consecutive pulse the amplitude increases, the decay is initially fast, but shows a long tail, the amplitude of which greatly increases with temperature. For the below-bandgap 2.3 eV (530 nm) LED excitation the photocurrent under illumination becomes progressively lower for each consecutive pulse, the signal overshoot under illumination is most pronounced for the first illumination pulse, and the signal decay under illumination becomes progressively slower for later excitation pulses.
The results of differentiating the photocurrent build-up and decay photocurrent by ln(t) for excitation with 4.8 eV (259 nm) LED and 2.3 eV (530 nm) LED are shown for the three temperatures in Fig. S4-S7 of the Supplementary Material. Here we illustrate the cases in point by presenting the data for the highest temperature of 380K in Fig. 7, 8. Fig. 7 illustrates the case

of 4.8 eV (259 nm) LED excitation and Fig. 8 shows the photocurrent build-up and decay for the 2.3 eV (530 nm) excitation (measurements performed at -10V, for convenience the signs on the current axes in the figures in are reversed). In the photocurrent build-up with 4.8 eV (259 nm) excitation three major processes, the fast initial increase with characteristic relaxation time 0.07 s, the slower increase preceding the photocurrent passing through the maximum (relaxation time of 23 s) and the long decay of photocurrent under illumination (relaxation time of 470 s). The peaks are broad, broader than expected for simple exponential build-up processes. The fast peak was difficult to quantitatively model. The slow peaks could be fitted with stretched exponents rather than simple exponents, and the broadening factor was β=0.5.

The photocurrent decay was initially fast, with characteristic decay time of 0.07 s close to the fast build-up time. This fast decay region was followed by a long tail with characteristic time close to 53 s, again well described by the stretched exponent with β=0.5.

With 2.3 eV (530 nm) LED excitation (Fig. 8), the behavior of the photocurrent build-up was similar to the 4.8 eV case. There still existed a fast build-up with characteristic time 0.13 s, a slower build-up with characteristic time of 36 s accurately approximated with the stretched exponent with the broadening constant β=0.5, and a long decay of the signal under illumination, with characteristic time constant more accurately estimated at the lowest temperature of 300K (Fig. 6, Fig. S5). Since the photocurrent steadily decreased for the 2.3 eV excitation for each consecutive pulse, it could be unambiguously estimated only for the first pulse at 300K where the relaxation time was 1350 s. The photocurrent decay showed a fast relaxation time of 0.09 s close to the fast build-up time and a slow tail with the characteristic decay time close to 60 s at 380K. This tail region could be accurately described by the stretched exponent model. The data are summarized in Table I. The studied temperature interval is too narrow and the number of points too small to be able to accurately obtain the temperature dependences of parameters involved, but for the fastest build-up and decay times for both types of excitations, it can be

positively stated that they are close to each other in both cases and characterized by similar activation energies of 0.16-0.18 eV, as shown for the build-up times in Fig. 9.

The Fermi level in the devices is pinned in the dark at E_c-0.8 eV, in the vicinity of the dominant deep trap. The deep centers in α-Ga_2O_3 have not been accurately mapped either experimentally or theoretically. The centers in question have been observed in DLTS spectra of lightly Sn doped α-Ga_2O_3 [23,24] and in PICTS spectra of undoped films [24]. Theoretical analysis [36] suggests that, under O-rich conditions and the Fermi level located in the upper half of the bandgap, the defect with the lowest formation energy and the level E_c-0.8 eV is the divacancy V_{Ga}-V_O with the highest filled acceptor level near E_c-0.8 eV or the O_{2i} interstitial with the highest acceptor level also near E_c-0.8 eV. Photocurrent spectra measurements in Fig. 2 additionally point to the important role of deep centers with optical ionization energies 2.3 eV and 3.1 eV. The former could be due to the Ga vacancy V_{Ga}^{3-} acceptor state, the latter –to one of the split interstitial donor states O_{i1} or O_{i2} [37]. The centers in have also been observed in doped α-Ga_2O_3 and for the 2.3 eV centers and they possess a barrier for capture of electrons and could be responsible for the observed persistent photoconductivity and photocapacitance [24, 25].

The very high EQE>>1 of the detectors is indicative of the well-known phenomenon in photoconductors related to strong trapping of one type of carriers [37-30], in our case, holes. This leads to increased lifetime of the other type of charge carriers (electrons). These electrons circulate in the circuit and contribute to photocurrent till the trapped carriers are released and made available for recombination. Under these conditions the photocurrent amplification is roughly determined by the ratio of the lifetime τ to the transit time, τ/t_{tr}, $t_{tr}=L/V_{dr}$, where L is the distance between the contacts and the drift velocity $V_{dr}=\mu E$ (μ being the effective mobility, E the electric field) [38-40]. For long lifetime and short transit times, this amplification accounts for high values of EQE. Decreasing the distance between the contacts or increasing the applied electric field should decrease the transit time and increase the photosensitivity and EQE. This is indeed observed for our α-Ga_2O_3 photodetector (see Fig. S1, S2, S3). In our case, the trapped

carriers are holes, the carriers circulating in the circuit and providing the high photocurrent are electrons.

For centers with a barrier for capture of electrons, such as the 2.3 eV optical threshold centers, we attribute to V_{Ga}^{3-} acceptors, there is no need for the presence of additional trapping centers because the electrons, once excited from these states, will be persistent until the recombination barrier is overcome [33, 34]. However, in this case, once the center has been excited it cannot return to the starting state for a long time. Therefore, prolonged illumination or a train of illumination pulses with fixed length will lead to the gradual decrease of the saturation photocurrent, as in our case with 2.3 eV (530 nm) excitation. This would not necessarily be the case if the hole traps responsible for high EQE are not the ones from which the carriers are excited. Then prolonged illumination or using of a train of repeated pulses will gradually increase the saturation current because of the build-up of the number of trapped holes.
One can also point out the fact that the relaxation curves we observe are stretched exponents rather than simple exponents. This is the hallmark of the current transport in the presence of centers with the barrier for capture of electrons and/or of prominent potential fluctuations [33-35]. Building a detailed model of recombination in semi-insulating α-Ga_2O_3 photoconducting detectors requires additional study, but it seems clear the very high photosensitivity and giant EQE of such photodetectors are the consequence of hole trapping and inherently goes hand in hand with the long relaxation times. Growth under Ga-rich conditions suppressing the formation of V_{Ga} could be conducive to alleviating the hole trapping effects but might make it more difficult to achieve high resistivity and low leakage current because of the enhanced contribution of Ga interstitials donors [36].

CONCLUSIONS

Interdigitated photoconducting detector on undoped α-Ga_2O_3 grown on sapphire and show high photosensitivity peaked at 235 nm wavelength and very high EQE around 100000, but long photocurrent build-up and decay times. The main centers present are E_c-0.8 eV defects on which

the Fermi level in the dark is pinned, deep acceptors with optical ionization threshold 2.3 eV and 3.1 eV, and deep traps with levels at E_c-0.25 eV, E_c-0.35 eV, E_c-0.5 eV, E_c-0.6 eV, visible either in TSC or in PICTS spectra.

Measurements of photosensitivity, EQE, EBIC signal as a function of applied bias suggest the high photosensitivity is due to hole trapping, thus enhancing the photocurrent due to photoelectrons. The centers responsible for hole trapping under the 2.3 eV LED illumination are most likely the centers with a barrier for capture of electrons and with optical ionization threshold at 2.3 eV.

The processes of photocurrent build-up and decay are characterized by fast transients with ~100 ms length similar for the build-up and the decay relaxations and for illumination with 2.3 eV and 4.8 eV light. For all relaxation processes the waveform of transitions is described by stretched exponents, which is a clear indication of the current flow in the presence of centers with a barrier for recombination of electrons and/or of pronounced potential fluctuations.

Acknowledgments

The work at NUST MISiS was supported in part by the Russian Science Foundation, grant no. 19-19-00409. The authors gratefully acknowledge Dr. M.B. Sheglov's help with x-ray measurements. Work performed as part of Interaction of Ionizing Radiation with Matter University Research Alliance (IIRM-URA), sponsored by the Department of the Defense, Defense Threat Reduction Agency under award HDTRA1-20-2-0002. The content of the information does not necessarily reflect the position or the policy of the federal government, and no official endorsement should be inferred. The work at UF was also supported by NSF DMR 1856662.

Author Declarations

The authors have no conflicts to disclose.

Availability of data

Data available on request from the authors. The data that support the findings of this study are available from the corresponding author upon reasonable request.

REFERENCES

[1] Gallium Oxide: Materials Properties, Crystal Growth, and Devices, ed. Masataka Higashiwaki and Shizuo Fujita (Springer Series in Materials Science ISBN 978-3-030-37152-4 ISBN 978-3-030-37153-1, 2020).

[2] D. Kaur and M. Kumar, A Strategic Review on Gallium Oxide Based Deep-Ultraviolet Photodetectors: Recent Progress and Future Prospects, Adv. Optical Mater., 9, 2002160 (2021).

[3] H. Deng, K.J. Leedle, Y. Miao, D.S. Black, K.E. Urbanek, J. McNeur, M. Kozák, A, Ceballos, P. Hommelhoff, O. Solgaard, R.L. Byer and J.S. Harris, Gallium Oxide for High-Power Optical Applications, Adv. Optical Mater. 8, 1901522 (2020).

[4] Jingan Zhou, Hong Chen, Kai Fu and Yuji Zhao, Gallium oxide-based optical nonlinear efects and photonics devices, J. Materials Research 36, 4832 (2021).

[5] Yuichi Oshima and Elaheh Ahmadi, Progress and challenges in the development of ultra-wide bandgap semiconductor α-Ga_2O_3 toward realizing power device applications, Appl. Phys. Lett. 121, 260501 (2022).

[6] S. J. Pearton, Fan Ren, Marko Tadjer, and Jihyun Kim, Perspective: Ga_2O_3 for ultra-high power rectifiers and MOSFETS, J. Appl. Phys. 124, 220901 (2018).

[7] J. Xu, W. Zheng and F. Huang. Gallium oxide solar-blind ultraviolet photodetectors: a review, J. Mater. Chem. C, 7, 8753 (2019).

[8] Xuanhu Chen, Fangfang Ren, Shulin Gu, and Jiandong Ye, Review of gallium-oxide-based solar-blind ultraviolet photodetectors, Photonics Research Vol. 7, 381 (2019).

[9] Elaheh Ahmadi, and Yuichi Oshima, Materials issues and devices of α- and β-Ga_2O_3, J. Appl. Phys. 126, 160901 (2019).

[10] Loh Kean Ping, Dilla Duryha Berhanuddin, Abhay Kumar Mondal, P. Susthitha Menon, Mohd Ambri Mohamed, Properties and perspectives of ultrawide bandgap Ga_2O_3 in optoelectronic applications, Chinese J. Physics, 73, 195 (2021).

[11] M. Higashiwaki, β-Ga_2O_3 material properties, growth technologies, and devices: a review, AAPPS Bull. 32, 3 (2022).

[12] Zeyu Chi, Jacob J. Asher, Michael R. Jennings,Ekaterine Chikoidze, and Amador Pérez-Tomás, Ga_2O_3 and Related Ultra-Wide Bandgap Power Semiconductor Oxides: New Energy Electronics Solutions for CO_2 Emission Mitigation, Materials 15, 1164 (2022).

[13] Qin Yuan, Long Shibing, Dong Hang, He Qiming, Jian Guangzhong, Zhang Ying, Hou Xiaohu, Tan Pengju, Zhang Zhongfang, Lv Hangbing, Liu Qi, Liu Ming, Review of deep ultraviolet photodetector based on gallium oxide, Chinese Physics B, 28, 018501 (2019).

[14] Kentaro Kaneko, Shizuo Fujita, and Toshimi Hitora, A power device material of corundum-structured α-Ga_2O_3 fabricated by MIST EPITAXY technique, Japanese Journal of Applied Physics 57, 02CB18 (2018).

[15] Alexander Y. Polyakov, Vladimir I. Nikolaev, Eugene B. Yakimov, Fan Ren, Stephen J. Pearton, and Jihyun Kim, Deep level defect states in β-, α-, and ε-Ga_2O_3 crystals and films: Impact on device performance, J. Vac. Sci. Technol. A 40, 020804 (2022).

[16] Anisha Kalra, Usman Ul Muazzam, R. Muralidharan, Srinivasan Raghavan, and Digbijoy N. Nath, The road ahead for ultrawide bandgap solar-blind UV photodetectors, J. Appl. Phys. 131, 150901 (2022).

[17] B. Qiao, Z. Zhang, X. Xie, B. Li, Kexue Li, Xing Chen, Haifeng Zhao, Kewei Liu, Lei Liu, Dezhen Shen, Quenching of persistent photocurrent in an oxide UV photodetector, J. Phys. Chem. C 2019, 123, 18516

[18] A.M. Armstrong, M.H. Crawford, A. Jayawardena, A. Ahyi and S.J. Dhar, Role of self-trapped holes in the photoconductive gain of β-gallium oxide Schottky diodes, J. Appl. Phys. 119, 103102 (2016).

[19] Yang Xu, Xuanhu Chen, Dong Zhou, Fangfang Ren, Jianjun Zhou, Song Bai, Hai Lu ,Shulin Gu, Rong Zhang, Youdou Zheng, and Jiandong Ye, Carrier Transport and Gain

Mechanisms in β –Ga_2O_3-Based Metal–Semiconductor–Metal Solar-Blind Schottky Photodetectors, IEEE Trans. Electron. Dev., 66, 2276, (2019).

[20] E.B. Yakimov, A.Y. Polyakov, I.V. Shchemerov, N.B. Smirnov, A.A. Vasilev, A.I. Kochkov, P.S. Vergeles, E.E. Yakimov, A.V. Chernykh, Minghan Xian, F. Ren, S.J. Pearton, On the nature of photosensitivity gain in Ga_2O_3 Schottky diode detectors: effects of hole trapping by deep acceptors, J. Alloys Compounds 879, 160394 (2021).

[21] X. Chen, F.-F. Ren, J. Ye and S. Gu, Gallium oxide-based solar-blind ultraviolet photodetectors, Semicond. Sci. Technol. 35, 023001(2020).

[22] Y. Qin, L. Li, X. Zhao, G.S. Tompa, H. Dong, G. Jian, Q. He, P. Tan, X. Hou, Z. Zhang, S. Yu, H. Sun, G. Xu, X. Miao, K. Xue, S. Long, M. Liu. Metal–Semiconductor–Metal ε-Ga2O3 Solar-Blind Photodetectors with a Record-High Responsivity Rejection Ratio and Their Gain Mechanism, ACS Photonics 7, 812 (2020).

[23] A. Y. Polyakov, V. I. Nikolaev, S. I. Stepanov, A. I. Pechnikov, E. B. Yakimov, N. B. Smirnov, I. V. Shchemerov, A. A. Vasilev, A. I. Kochkova, A.V. Chernykh, and S. J. Pearton, Electrical Properties and Deep Traps in α-Ga2O3:Sn Films Grown on Sapphire by Halide Vapor Phase Epitaxy, ECS J Solid State Sci. Techn,, 9, 045003 (2020).

[24] A. Y. Polyakov, N. B. Smirnov, I. V. Shchemerov, E. B. Yakimov, V. I. Nikolaev, S. I. Stepanov, A. I. Pechnikov, A. V. Chernykh, K. D. Shcherbachev, A. S. Shikoh, A. Kochkova, A. A. Vasilev, and S. J. Pearton, Deep trap spectra of Sn-doped α-Ga_2O_3 grown by halide vapor phase epitaxy on sapphire, APL Mater. 7, 051103 (2019)

[25] Alexander Y. Polyakov, Vladimir I. Nikolaev, Igor N. Meshkov, Krzysztof Siemek, Petr B. Lagov, Eugene B. Yakimov, Alexei I. Pechnikov, Andrey G. Kobets, Sergey I. Stepanov, Ivan V. Shchemerov, Anton A. Vasilev, Alexey V. Chernykh, Anton A. Losev, Alexandr D. Miliachenko, Igor A. Khrisanov, Yu.S. Pavlov, U.A. Kobets and Stephen J. Pearton, Point defect creation by proton and carbon irradiation of α-Ga_2O_3, J. Appl. Phys. 132, 035701 (2022).

[26] Dieter K. Schroder, Semiconductor Materials and Device Characterization (John Wiley and Sons, New York, 1990), chapter 7

[27] M. Tapiero, N. Benjelloun, J.P. Zielinger, S. El Hamd, and C. Noguet, Capacitance temperature analysis of midgap states in hydrogenated amorphous silicon, J. Appl. Phys. 54, 4006 (1988)

[28] O. V. Smolin, E. V. Susov, and E. B. Yakimov, EBIC characterization of HgCdTe based photoconductive elements, Proc. SPIE, 5834, 242 (2005).

[29] V. V. Krapukhin, P. S. Vergeles, and E. B. Yakimov, Simulation and measurements of EBIC images of photoconductive elements based on HgCdTe, Semiconductors,41, 407 (2007).

[30] E. B. Yakimov, A. Y. Polyakov, N. B. Smirnov, I. V. Shchemerov, Jiancheng Yang, F. Ren, Gwangseok Yang, Jihyun Kim, and S. J. Pearton , "Diffusion length of non-equilibrium minority charge carriers in β-Ga_2O_3 measured by electron beam induced current", Journal of Applied Physics 123, 185704 (2018)

[31] A. Y. Polyakov, N. B. Smirnov, 1 I. V. Schemerov,1 A. V. Chernykh, E. B. Yakimov, A. I. Kochkova, A. N. Tereshchenko, and S. J. Pearton, Electrical Properties, Deep Levels and Luminescence Related to Fe in Bulk Semi-Insulating β-Ga_2O_3 Doped with Fe, ECS J. Sol State Sci. Technol, 8**,** Q3091 (2019).

[32] A. Y. Polyakov, N. B. Smirnov, I. V. Shchemerov, E. B Yakimov, S. J. Pearton, Fan Ren, A. V. Chernykh, D. Gogova, and A. I. Kochkova, Electrical Properties, Deep Trap and Luminescence Spectra in Semi-Insulating, Czochralski β-Ga2O_3 (Mg), ECS J. Solid State Sci. Technol., 8 (7) Q3019 (2019).

[33] A. Dissanayake, M. Elahi, H. X. Jiang and J.Y. Lin, Kinetics of persistent photoconductivity in $Al_{0.3}Ga_{0.7}As$ and $Zn_{0.3}Cd_{0.7}Se$ semiconductor alloys, Phys. Rev. B 45, 13996 (1992).

[34] J. Y. Lin, A. Dissanayake, G. Brown, and H. X. Jiang, Relaxation of persistent photoconductivity in Al0.$_3$$Ga_{0.7}As$, Phys. Rev. B 42, 5855 (1990).

[35] A.Y. Polyakov, N.B. Smirnov, I.V. Shemerov, In-Hwan Lee, Taehoon Jang, A.A. Dorofeev, N.B. Gladysheva, E.S. Kondratyev, Y.A. Turusova, R.A. Zinovyev, A.V. Turutin, F. Ren, and S.J. Pearton, Current Relaxation Analysis in AlGaN/GaN High Electron Mobility Transistors ,J. Vac. Sci. Technol. B 35, 011207 (2017).

[36] E. B. Yakimov, A. Y. Polyakov, I. V. Shchemerov, N. B. Smirnov, A. A. Vasilev, P. S. Vergeles, E. E. Yakimov, A. V. Chernykh, F. Ren, and S. J. Pearton, Experimental estimation of electron–hole pair creation energy in β-Ga_2O_3**,** Appl. Phys. Lett. 118, 202106 (2021).

[37] Takuma Kobayashi, Tomoya Gake, Yu Kumagai, Fumiyasu Oba and Yu-ichiro Matsushita, Energetics and electronic structure of native point defects in α-Ga_2O_3, Applied Physics Express 12, 091001 (2019).

[38] S.M. Ryvkin, Photoelectric Effects in Semiconductors (Consultants Bureau, New York, 1964).

[39] J.S. Blakemore, Semiconductor Stattistics (Pergamon, New York, 1962)

[40] A. Rose, Concepts in photoconductivity and allied problems (Interscience publishers, New York, 1963).

Table I. Characteristic relaxation times

Process	300K		340K		380K	
	259 nm	530 nm	259 nm	530 nm	259 nm	530 nm
Build-up	1)0.46 s(broad) 2)37 s (stretched, b=0.5) 3)330 s (β=0.5)	1)0.85 s(broad) 2)36 s (stretched, β=0.5) 3)1350 s (stretched, β=0.5)s	1)0.22 s (broad) 2)35 s (stretched, β=0.5) 3)381 s (stretched,β=0.5)	1)0.23 s (broad) 2)37 s (stretched, β=0.5) 3)1200 s (stretched, β=0.5)	1)0.07 s (broad) 2)33 s (stretched, b=0.5) 3)420 s (stretched, β=0.5)	1)0.13 s (broad) 2)36 s(stretched, β=0.5) 3)1100 s (stretched, β=0.5)
Decay	1)0.2 s(broad)	1)0.2 s(broad)	1)0.1s(broad) 2)220s (Stretched, β=0.5)	1)0.1s (broad)	1)0.07 s (broad) 2)53s (Stretched, β=0.5)	1)0.09 s (broad) 2)60s (Stretched, β=0.5)

Figure Captions

Fig. 1. Photograph of the fabricated photodetector structure showing characteristic dimensions.

Fig. 2. (Color online) (a)Room temperature I-V characteristics measured in the dark (black line)and with illumination with LEDs with peak photon wavelengths of 940 nm (solid magenta line), 840 nm (dashed magenta line), 660 nm (solid red line), 625 nm (dashed red line), 530 nm (olive line), 470 nm (dashed cyan line), 455 nm (cyan line), 400 nm (blue line), 385 nm (orange line), 365 nm (violet line), 277 nm (purple line); (b) photocurrent at 40V and -40V normalized by the dark current.

Fig. 3 (Color online) Current density measured at -40V after I-V spectra measurement at room temperature, cooling down at -40V, illumination with 259 nm LED for 5 min at 120K, heating up to 430K in the dark (red line), the same after cooling down at -40V in the dark (red line dashed); current density measured next day at -40V upon cooling to 150K in the dark after previously heating to 430K in the dark (blue line dashed), current at -40V measured after illumination with 259 nm LED at 150K (blue line).

Fig. 4 (Color online) PICTS spectrum measured at -10V, with LED excitation with peak wavelength 277 nm, pulse length 5s, time windows 400 ms/4000 ms.

Fig. 5. EBIC images with the probing beam accelerating voltage 25 kV and beam current 10 nA, (a) no applied bias, (b) applied bias of 10V, (c) applied bias of 20V, (d) the blow-up of image (c) with higher magnification; the scale is seen from the interdigital distance of 30 μm.

Fig. 6 (Color online) The photocurrent at -10V transients measured (a)-(c) with 530 nm LED excitation (green shading) and (d)-(f) with 259 nm LED excitation (pink shading) at temperatures 300K, 340K, 380K.

Fig. 7 (Color online) (a) the first derivative of photocurrent by Ln(t) for the photocurrent build-up at 380K with 259 nm LED excitation (the data shown for the three consecutive pulses analyzed; (b) the same for photocurrent decay.

Fig. 8. (Color online) (a) the first derivative of photocurrent by Ln(t) for the photocurrent build-up at 380K with 530 nm LED excitation (the data shown for the three consecutive pulses analyzed; (b) the same for photocurrent decay.

Fig. 9. (Color online) Arrhenius plots of tT^2 for photocurrent build up with 259 nm LED and 530 nm LED.

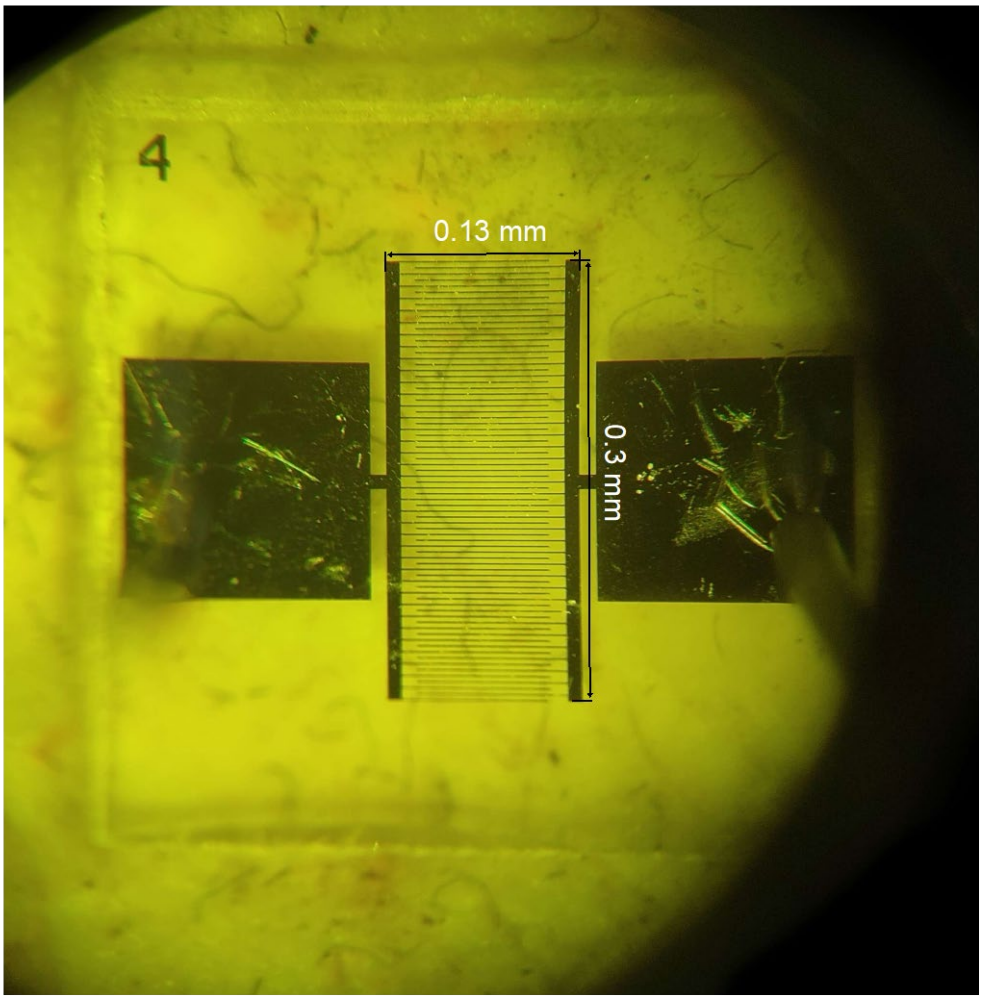
4
0.13 mm
0.3 mm

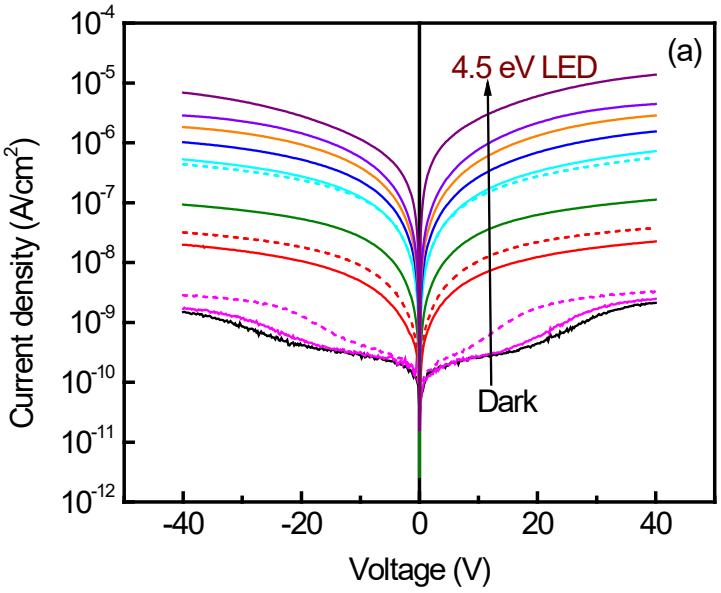
(a)
4.5 eV LED
Dark
Current density (A/cm^2)
Voltage (V)
10^{-4}
10^{-5}
10^{-6}
10^{-7}
10^{-8}
10^{-9}
10^{-10}
10^{-11}
10^{-12}
-40
-20
0
20
40

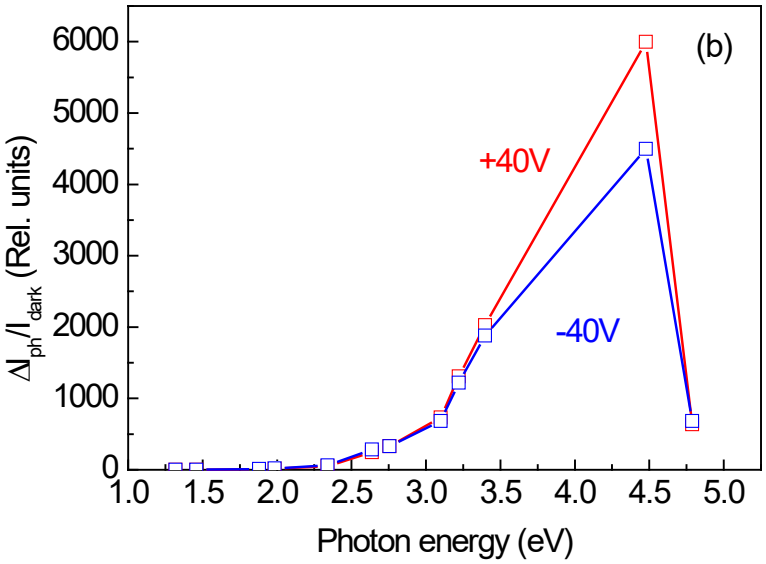
(b)
+40V
-40V
$\Delta I_{ph}/I_{dark}$ (Rel. units)
Photon energy (eV)
6000
5000
4000
3000
2000
1000
0
1.0
1.5
2.0
2.5
3.0
3.5
4.0
4.5
5.0

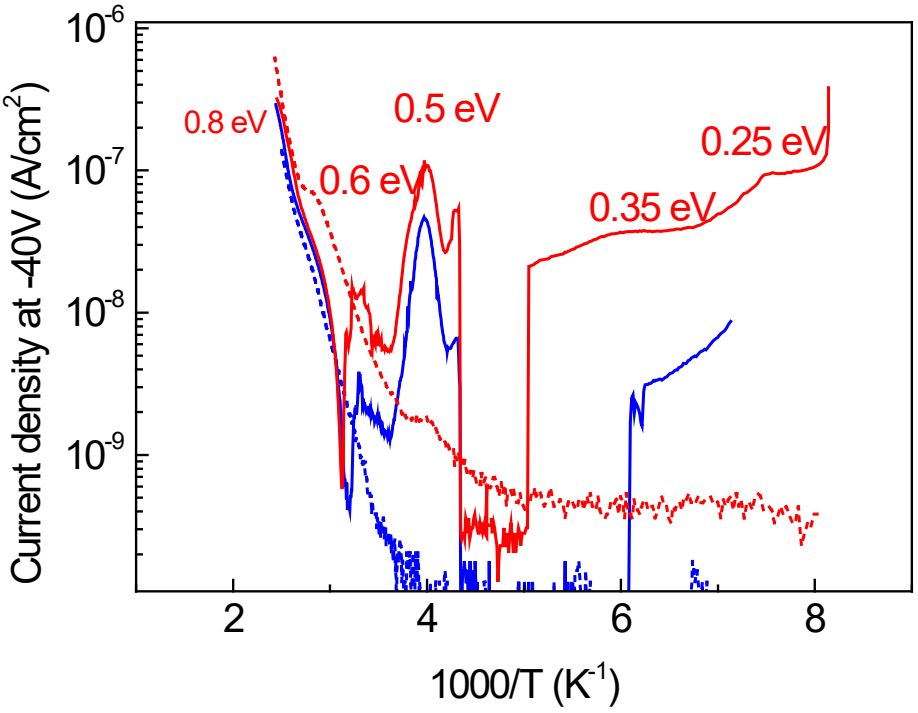
Current density at -40V (A/cm^2)
10^{-6}
10^{-7}
10^{-8}
10^{-9}
0.8 eV
0.6 eV
0.5 eV
0.35 eV
0.25 eV
2
4
6
8
1000/T (K^{-1})

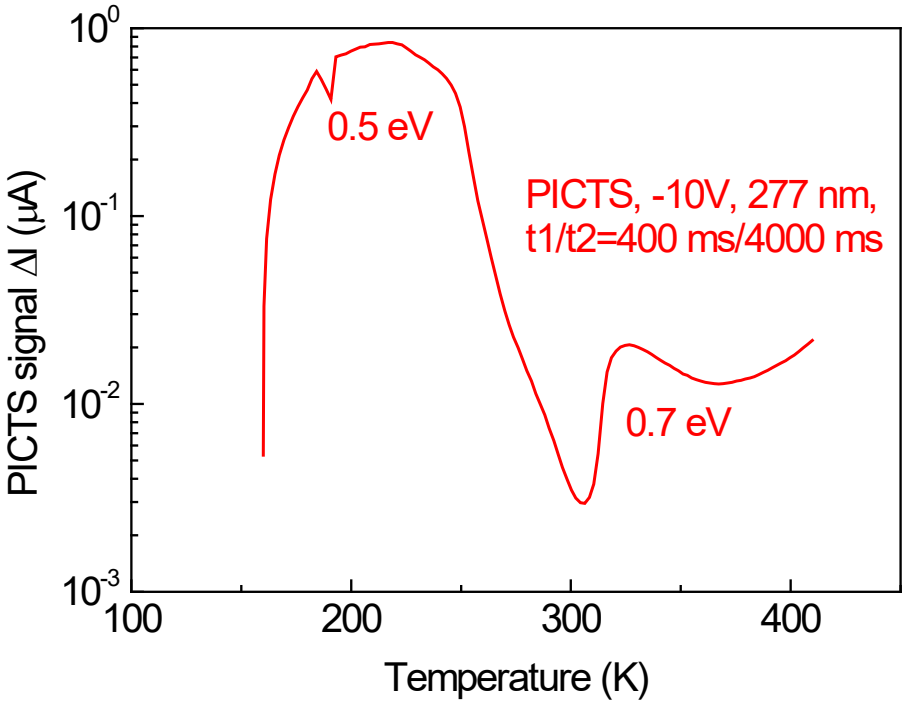
PICTS signal ΔI (μA)
10^0
10^-1
10^-2
10^-3
100
200
300
400
Temperature (K)
0.5 eV
0.7 eV
PICTS, -10V, 277 nm,
t1/t2=400 ms/4000 ms

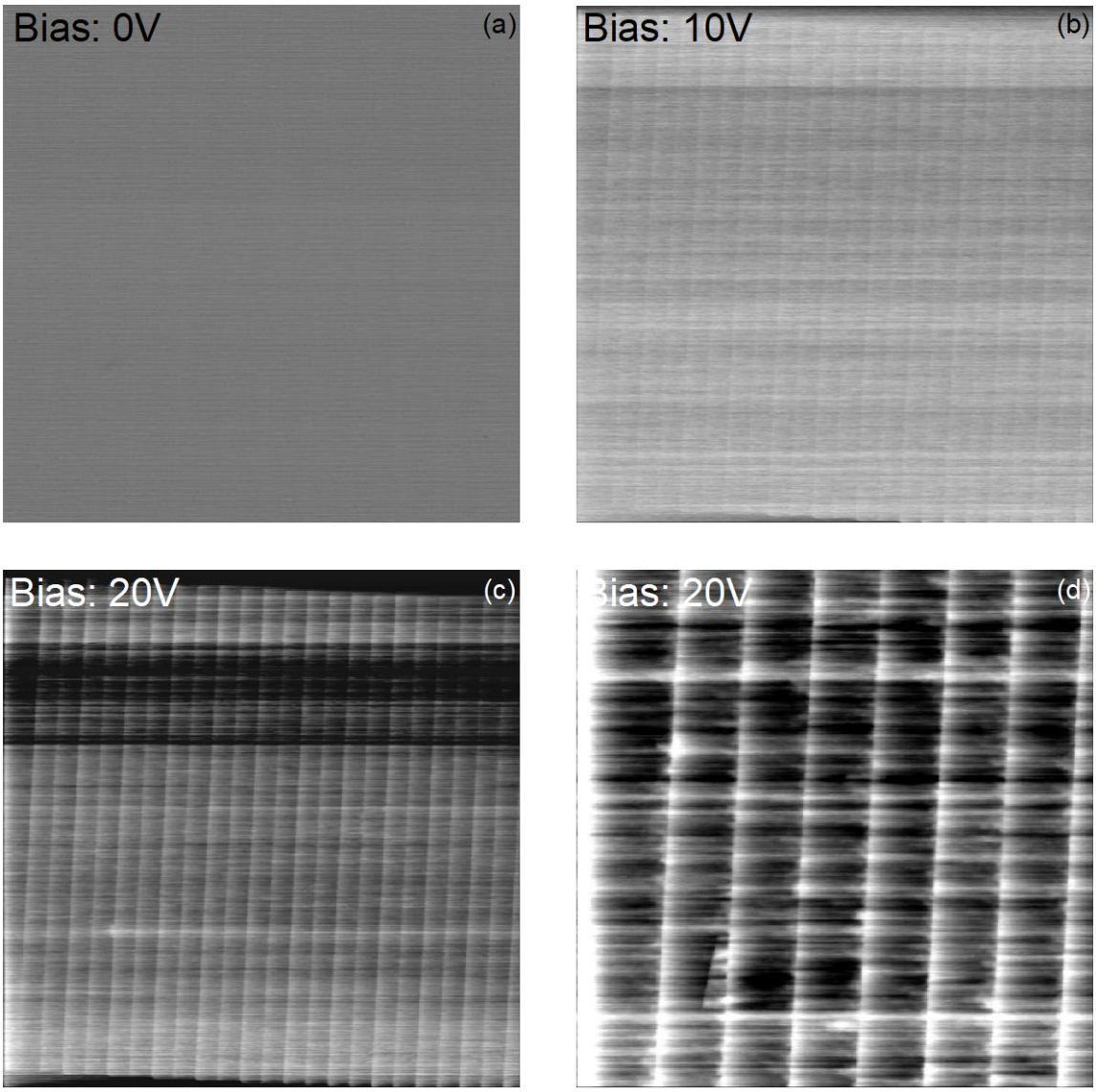
Bias: 0V
(a)
Bias: 10V
(b)
Bias: 20V
(c)
Bias: 20V
(d)

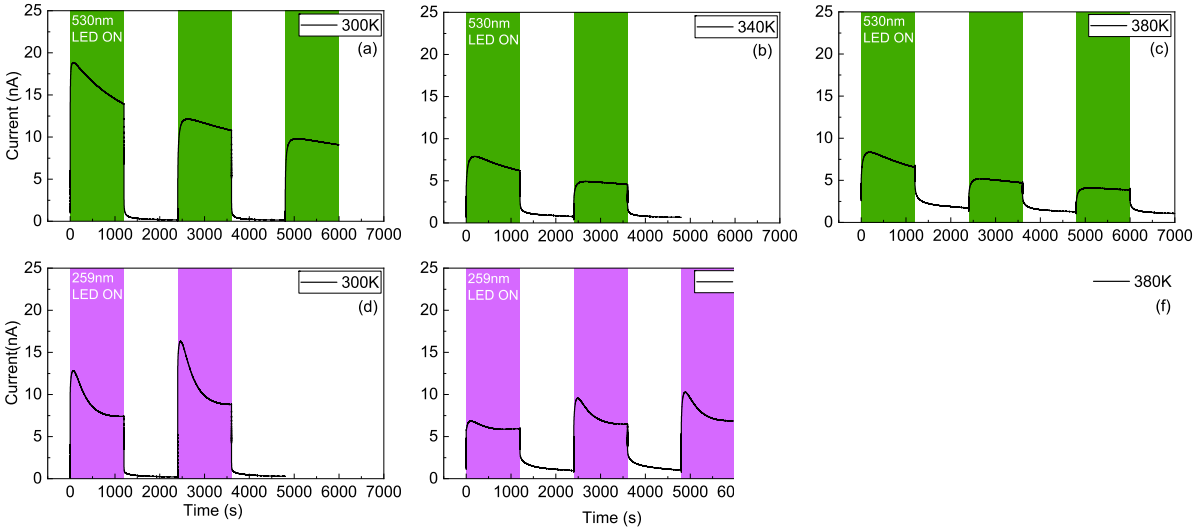
530nm
LED ON
300K
(a)
340K
(b)
380K
(c)
259nm
LED ON
(d)
(f)
Current (nA)
Current(nA)
Time (s)
0 1000 2000 3000 4000 5000 6000 7000
0 5 10 15 20 25

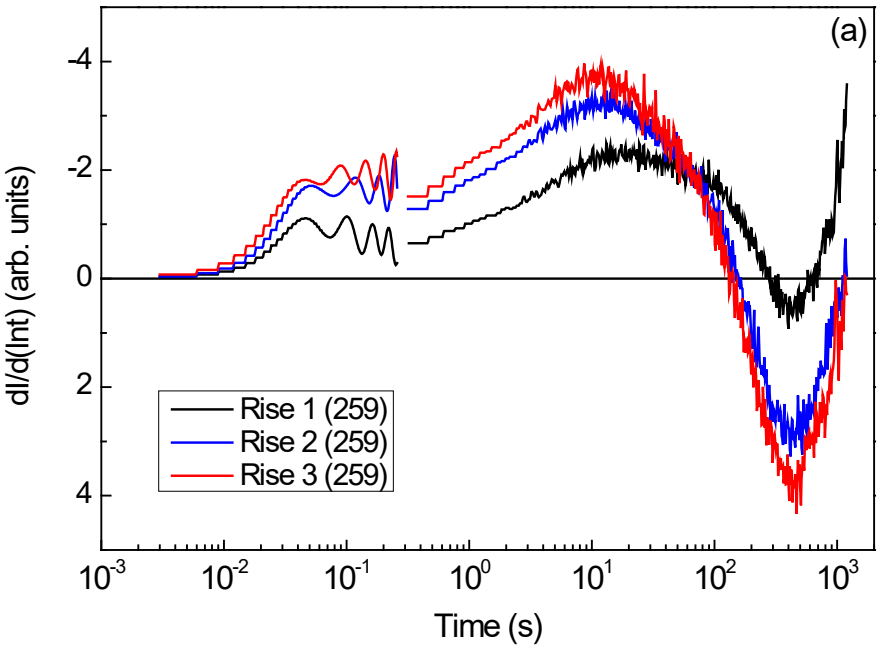
(a)
dI/d(lnt) (arb. units)
-4
-2
0
2
4
Rise 1 (259)
Rise 2 (259)
Rise 3 (259)
10-3
10-2
10-1
100
101
102
103
Time (s)

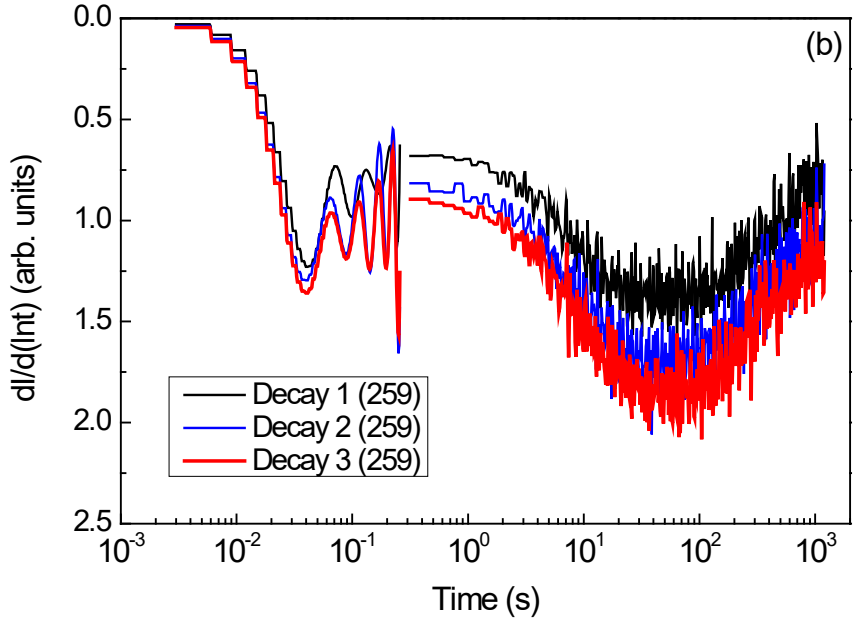
(b)
dI/d(lnt) (arb. units)
0.0
0.5
1.0
1.5
2.0
2.5
Decay 1 (259)
Decay 2 (259)
Decay 3 (259)
10-3
10-2
10-1
100
101
102
103
Time (s)

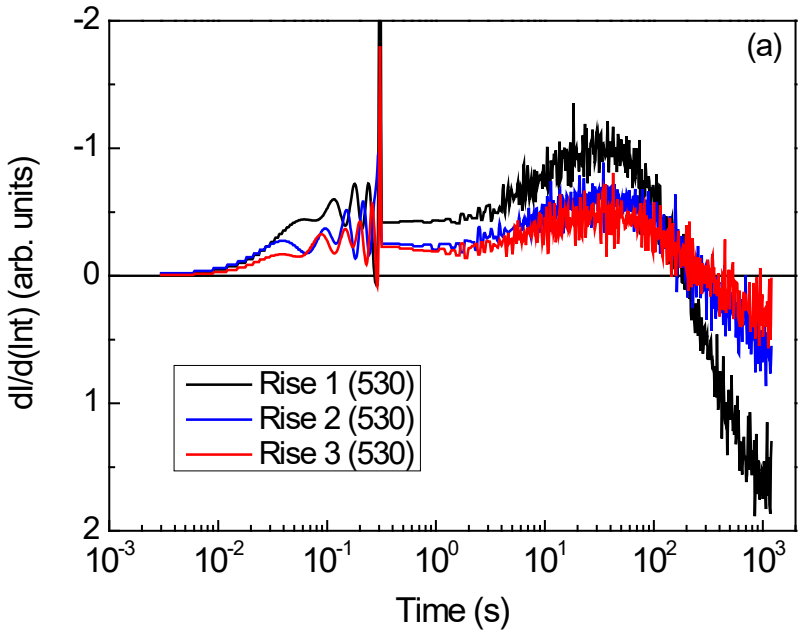
(a)
dI/d(lnt) (arb. units)
Time (s)
Rise 1 (530)
Rise 2 (530)
Rise 3 (530)

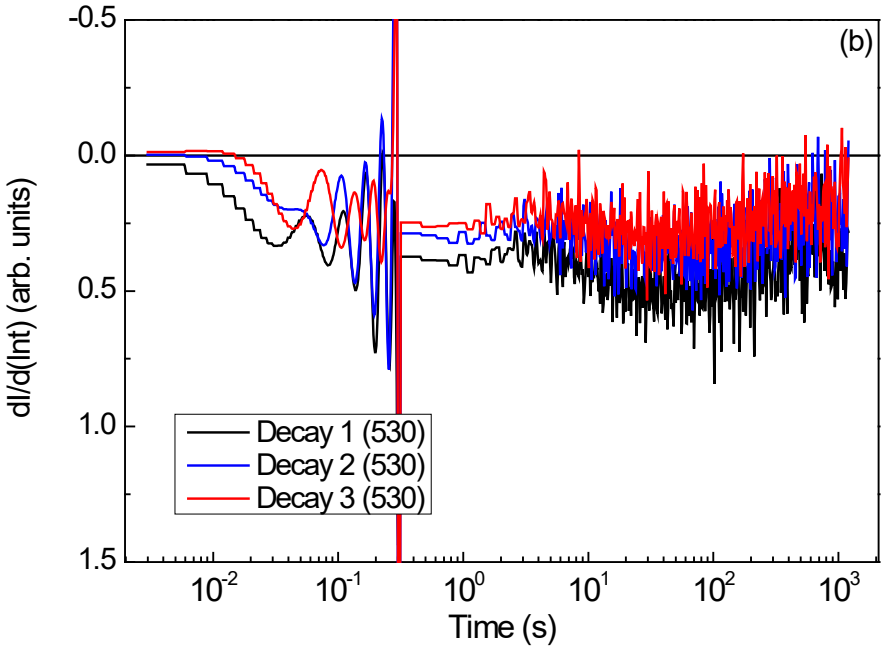
(b)
dI/d(lnt) (arb. units)
Time (s)
Decay 1 (530)
Decay 2 (530)
Decay 3 (530)

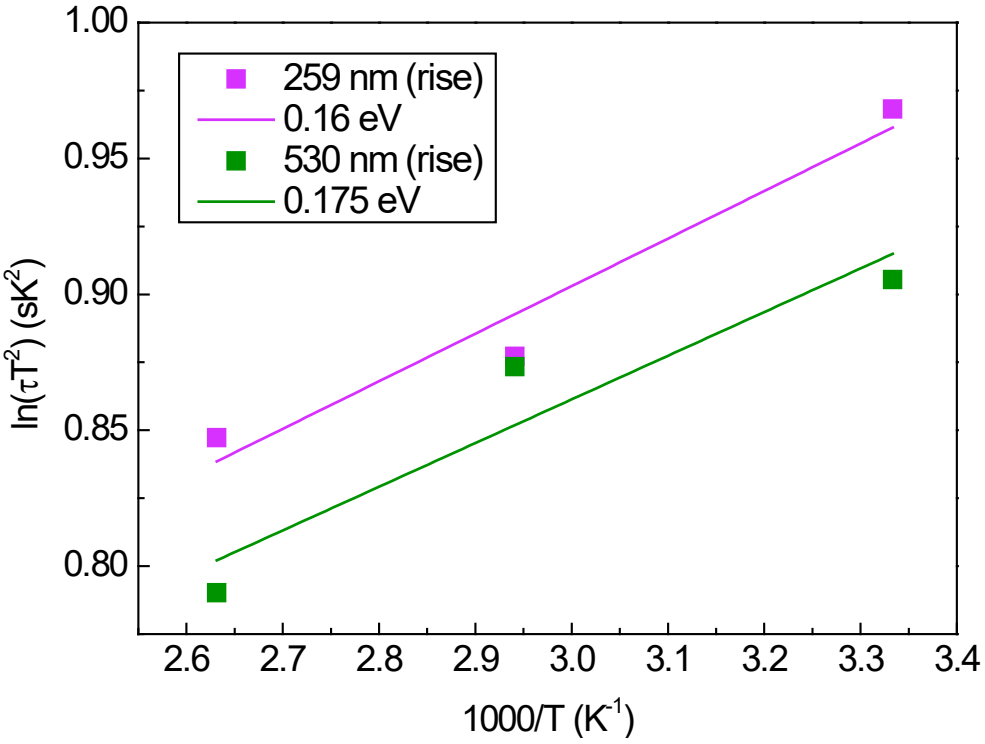
259 nm (rise)
0.16 eV
530 nm (rise)
0.175 eV
1.00
0.95
0.90
0.85
0.80
ln(τT²) (sK²)
2.6
2.7
2.8
2.9
3.0
3.1
3.2
3.3
3.4
1000/T (K⁻¹)